Chemically expanded graphite-based ultra-high molecular weight polyethylene composites with enhanced mechanical properties

Julian Somberg[a,*], Gil Gonçalves[b], María Soria Sánchez[c], Nazanin Emami[a]

[a] *Division of Machine elements, Luleå University of Technology, Luleå, Sweden*
[b] *Centre for Mechanical Technology and Automation (TEMA), Mechanical Engineering Department, University of Aveiro, 3810-193 Aveiro, Portugal*
[c] *Institute of Material Science of Barcelona, Barcelona, Spain*

Abstract

Chemically expanded graphite (CEG) has recently been identified as promising reinforcement for polymer composites with the ability for commercial up-scaling. In this work, silane and polydopamine functionalized CEG were successfully synthesized and employed to prepare ultra-high molecular weight polyethylene (UHMWPE) composites with an enhanced interfacial compatibility. Characterisation of the functionalized CEG indicated a significant oxygen reduction, which gave rise to a restoration of the graphitic structure. The polydopamine functionalized CEG showed an enhanced exfoliation and dispersion in organic solvents and the polymer matrix with respect to the non-modified CEG. The silane functionalized CEG provided a higher affinity towards the matrix with polymer chains covering the CEG sheets on the fracture surfaces. The addition of functionalized CEG enhanced the mechanical properties of the matrix with an increase in micro-hardness of up to 25% and storage modulus up to 58%. Furthermore, the hydrophobicity of the composites was significantly enhanced with an increase in water contact angle from 98.6° for the pure polymer to 119° for 5 wt% silane functionalized CEG. Preliminary wear experiments indicated the potential of the composites for tribological applications with a decrease in wear rate of up to 99% under water lubricated conditions.

Keywords: Chemically expanded graphite, UHMWPE, Dynamic Mechanical Analysis, Hydrophobicity, Wear

*Corresponding author. Tel. +46 920 491657. E-mail address: Julian.Somberg@ltu.se (J. Somberg)

1. Introduction

Graphene possesses a unique combination of properties such as a high mechanical strength and stiffness as well as a high electrical and thermal conductivity [1]. These properties make graphene a promising nano-scale reinforcement for polymer composites [2]. However, the full potential of graphene as reinforcement is not materialised due to the often weak interfacial interactions with the polymer matrix and poor dispersion within the matrix. Graphene is hydrophobic which makes the effective dispersion in polar solvents and matrices difficult. To enhance the dispersability, graphene oxide (GO) is often considered as alternative which can easily be dispersed in polar solvents and matrices due to presence of oxygen moieties [3].

Our previous work on GO / ultra-high molecular weight polyethylene (UHMWPE) composites presented a low fracture toughness of the materials which resulted from a weak interface between the reinforcement and non-polar polymer [4]. For non-polar polymers, including UHMWPE, bonding with GO relies on weaker van der Waals forces while the hydrophobic nature of UHMWPE furthermore interacts poorly with the highly polar GO [5, 6]. Therefore, it is expected that a lower oxygen content enables an enhanced interfacial bonding with the matrix. Reducing GO either thermally or chemically to obtain rGO provides an option to acquire near oxygen-free GO. However, re-aggregation through $\pi - \pi$ stacking and dispersion problems are inevitably re-introduced while lattice defects, introduced by the initial oxidation, significantly limit the mechanical properties of rGO [7, 8].

Work by Lin et al. on the scalable preparation of graphene has yielded chemically expanded graphite (CEG) with only a low degree of oxidation (oxygen content of around 15%) [9]. The expanded graphite lamella provided an open structure allowing for efficient exfoliation under mild conditions, while the low degree of oxidation prevents the extensive introduction of lattice defects[9]. In more recent work by Wang and co-authors [10], a surfactant was used to exfoliate CEG and obtain stable dispersions in water. Without surfactant, the dispersion proved to be difficult due to the low oxygen content of CEG, making it hydrophobic. The hydrophobic character of CEG make it a promising reinforcement for non-polar polymers. Recent work by de Oliveira Aguiar et al. furthermore showed promising results for the in-

corporation of CEG in UHMWPE [11].

For graphene/GO-polymer composites, functionalization is often considered to enhance the dispersion and interfacial interaction between the matrix and reinforcements [12]. Recent advancements have indicated the potential of functionalisation with polydopamine (PDA) and silane compounds as an effective method to increase the polymer-reinforcement interface. Dopamine mimics the adhesive proteins from mussels which have shown affinity with a wide variety of organic and inorganic surfaces [13, 14]. Under mild alkaline conditions, dopamine self-polymerises to form PDA through Michael addition or Schiff base reactions [15]. PDA readily bonds with different functional groups [16]. Silane agents have proven to be effective for the functionalization of graphene, graphite and respective derivates [17, 7, 18, 19]. By hydrolysis, silanol groups are obtained on the silane compound which readily bonds with the hydroxyl groups present on the carbon lattice trough a condensation reaction. [20, 21]. Wang et al. presented a 400% increase in storage modulus of Poly(methyl methacrylate) (PMMA) at 10wt% [3-(Methacryloyloxy)propyl]trimethoxysilane (MPS) functionalized CEG, with respect to a 208% increase for non-functionalized CEG. MPS grafting enhanced the exfoliation behaviour of CEG, although also reducing the wetting behaviour to polar solvents[22].

The above mentioned literature has highlighted the potential for CEG to be used as reinforcement in non-polar polymer composites. In this work, novel UHMWPE composites based on CEG were prepared at three different reinforcement contents. To enhance the dispersion and interfacial adhesion with the polymer, CEG functionalized with PDA and MPS and their respective composites were synthesized and characterized. The dispersability and interfacial compatibility of CEG and functionalized CEG (f-CEG) were examined. Furthermore, the thermomechanical and surface properties were obtained with respect to prospective use of these composite materials in bearing applications.

2. Experimental

2.1. Materials

Commercial expandable graphite (+50 mesh) was obtained from Sigma Aldrich. Ethanol 96% was obtained from Solveco AB, Sweden. Tris, Tris HCl, [3-(Methacryloyloxy)propyl] trimethoxysilane (MPS) 98%, dopamine hydrochloride 98% and N-Methyl-2-pyrrolidone (NMP) 99% were supplied by Sigma Aldrich. UHMWPE (MIPELON XM-220) was supplied by Mitsui Chemicals, Japan with a molecular weight of 200 x 10^4 g mol $^{-1}$ and a particles size of 30 µm.

2.2. Preparation and functionalization of CEG

Chemically expanded graphite was synthesized according to the method described in work by Peng et al. [23] and is illustrated in figure 1. To obtain the intermediate graphite intercalation compound (GIC), 4 g of expandable graphite flakes were added to 160 ml of concentrated H_2SO_4 (98%), keeping the solution in an ice bath to avoid excessive heat release. Following, 4 g of $KMnO_4$ was added to the mixture and stirred during 1 hour at room temperature and subsequently filtered and washed with H_2SO_4, obtaining the dark green GIC. Separately, 360 ml of H_2SO_4 (98%) and 40 mL of H_2O_2 (30%) were mixed in a beaker immersed in an ice bath, where the GIC was added while stirring during 10 min. Thereafter, the mixture was left standing overnight and filtered and washed with deionized water to finally obtain CEG.

To prepare PD-CEG, 0.1 g CEG was ultrasonically exfoliated in 50 ml ethanol for 30 min. 300 ml 0.1M tris buffer solution was prepared and adjusted to pH 8.5. The buffer solution was then transferred to a round bottom flask equipped with a magnetic stirrer and reflux condenser. 0.05 g dopamine hydrochloride was consequently added an stirred until the solution turned slightly pink indicating polymerization of the dopamine. The CEG suspension was then added and the solution heated to 60°C for 24 hours while continuously stirring the solution. After the solution was cooled back to room temperature, it was vacuum filtrated using a 0.22 µm PVDF membrane filter before repeatedly washing and filtering with ethanol and consequently re-dispersing the PDA-CEG in ethanol.

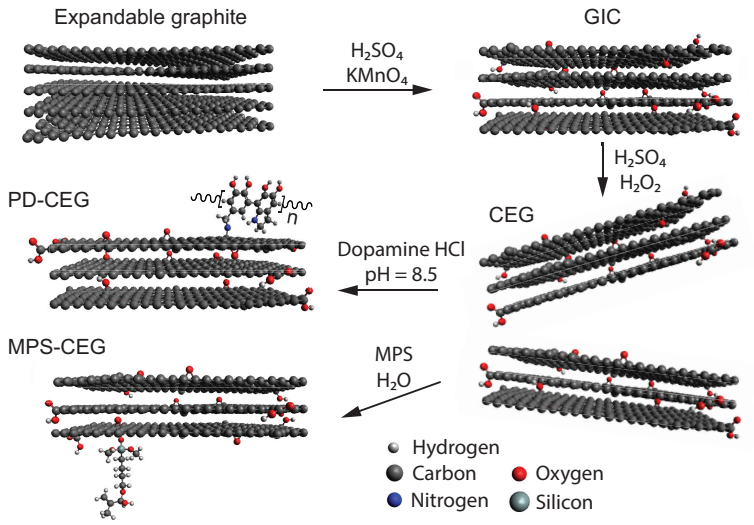

Figure 1: Illustration of the synthesis and functionalization of CEG

MPS functionalization of CEG was performed using a modified version of the method described by Yuan et al. [24]. 0.1 g of CEG was ultrasonically dispersed in 200 ml ethanol for 30 min after adjusting the pH to 3.5 by diluted hydrochloric acid. The mixture was consequently transferred to a round bottom flask with reflux condenser and heated to 70°C under constant magnetic stirring. The 0.5 g MPS was then dissolved in 50 ml ethanol and dropwise added to the CEG mixture and left to react for 24 hours. The cooled down solution was repeatedly washed and filtered using a PVDF filter and the MPS-CEG re-dispersed in ethanol.

2.3. Manufacturing of UHMWPE composites

Based on the initial quantity of used CEG, the volume of CEG/f-CEG dispersions to obtain the concentrations of 1, 3 and 5 wt% was determined. The composites were prepared by sonication of the dispersions for 60 min before adding 10 g of UHMWPE and a consequent 60 minute sonication step. The mixture was then mixed by planetary ball milling (PM-100, Retsch) at 200 rpm for 120 min. The obtained slurry was oven dried for 24 hours at 60°C before consolidating the acquired powder by means of compression moulding. The compression moulding was done at 190°C using several 15 MPa loading and unloading cycles.

2.4. Characterisation of CEG and f-CEG

Raman spectroscopy was used to analyse the characteristic carbon peak of CEG and highlight changes arrising from the functionalization. The experiments were executed using an Xplora plus Raman microscope (Horiba Scientific, NJ, USA). A 532 nm laser was used at 10 mW over a range of 300-3900 cm^{-1}. Fourier transform infrared spectroscopy (FTIR) was performed on the pure CEG and f-CEG powders to identify bonds related to the introduced functional groups. The dispersions were dried at 60 °C and the obtained powders were ground and pressed into KBr pellets. The measurements were performed using a Vertex 70v FTIR spectrometer (Bruker, MA, USA) over a frequency range of 500-4000 cm^{-1}. X-ray photoelectron spectroscopy (XPS) was performed on the CEG powders using a Axis Ultra DLD XPS spectrometer (Kratos Analytical Ltd., UK) using a Al kα x-ray source. X-ray diffraction (XRD) studies were performed on the CEG species using an Empyrean diffractometer (PANanalytical, the Netherlands) equipped with a Cu kα x-ray source. Furthermore, thermogravimetric analysis (TGA) was performed on CEG and f-CEG using a TGA 8000 (Perkin Elmer, MA, USA). The powders were heated under nitrogen atmosphere from room temperature to 800°C employing a heating rate of 10°C min^{-1}.

2.5. Characterisation of polymer composites

The dispersion of the reinforcements within the matrix and the interfacial adhesion between reinforcement and polymer were analysed. Both the powder mixtures before compression moulding and cryogenic fracture surfaces of the consolidated materials were imaged using a Magellan 400 scanning electron microscope (SEM) (FEI company, OR, USA). Differential scanning calorimetry (DSC) was used to investigate the effect of the different reinforcements on the polymer thermal and crystallisation behaviour. Experiments were executed using a DSC821 instrument (Mettler Toledo, OH, USA) under an inert nitrogen atmosphere. The 6-8 mg samples were heated to 200°C and held isothermally for 5 min. The pans were then cooled to -130°C and heated to 200°C at a heating rate of 10°C min^{-1}. Dynamic mechanical analysis (DMA) was used to determine the viscoelastic behaviour of the composites by employing a Tritec 2000 DMA (Triton Technologies, UK). Samples were machined to dimensions of 25x3.5x4 mm and subjected to three-point-bending over a temperature range from -150°C

to 170°C at a heating rate of 2°C min^{-1} and a frequency of 1 Hz and 10 Hz. Using the DMA curves, the reinforcement factor, r, was determined for a given reinforcement content using equation 1 [25]. In this equation, E_c is the composite storage modulus, E_m is the pure matrix storage modulus and V_f is the reinforcement volume fraction. Due to the inability to accurately determine the CEG/f-CEG, the mass fraction was used instead.

$$r = \frac{(E_c/E_m - 1)}{V_f} \tag{1}$$

Additionally, the adhesion factor, A, was determined for the reinforcements using equation 2 [25]. The adhesion factor describes the damping of the material relative to the reinforcement volume fraction. In this equation $tan\ \delta_c$ and $tan\ \delta_m$ represent the damping factor of the composite and matrix, respectively. The damping effect by the reinforcement and interphase is considered negligible.

$$A = \frac{1}{1 - V_f} \frac{tan\ \delta_c}{tan\ \delta_m} - 1 \tag{2}$$

The effect of the used reinforcements on the surface mechanical properties was investigated through micro hardness indentations. The micro hardness was evaluated using a MXT-α (Matsuzawa, Japan) Vickers hardness indenter with a load of 100 g for 20 seconds. Ten indentations were made for each material. The wettability of the surface was analysed by contact angle measurement by depositing 4 µl drops of distilled water using an Attension optical tensiometer (Biolin Scientific, Sweden). Di-iodomethane was furthermore used to calculate the surface free energy (SFE) using the OWRK theory. For each material a minimum ten drops were analysed per liquid. To investigate the potential of these materials for bearing applications, an initial tribological characterisation was executed using a Cameron-plint TE77 reciprocating tribometer under water lubricated conditions. The materials were machined to pins of 4.1x4.1mm and slid against SS2333 stainless steel counter surfaces at a stroke length of 5 mm with a roughness of 0.3 µm Ra. A contact pressure of 10 MPa was used and a sliding speed of 0.02 ms^{-1} over the total test duration of 40 hours.

3. Results and Discussion

3.1. Characterisation of CEG and f-CEG

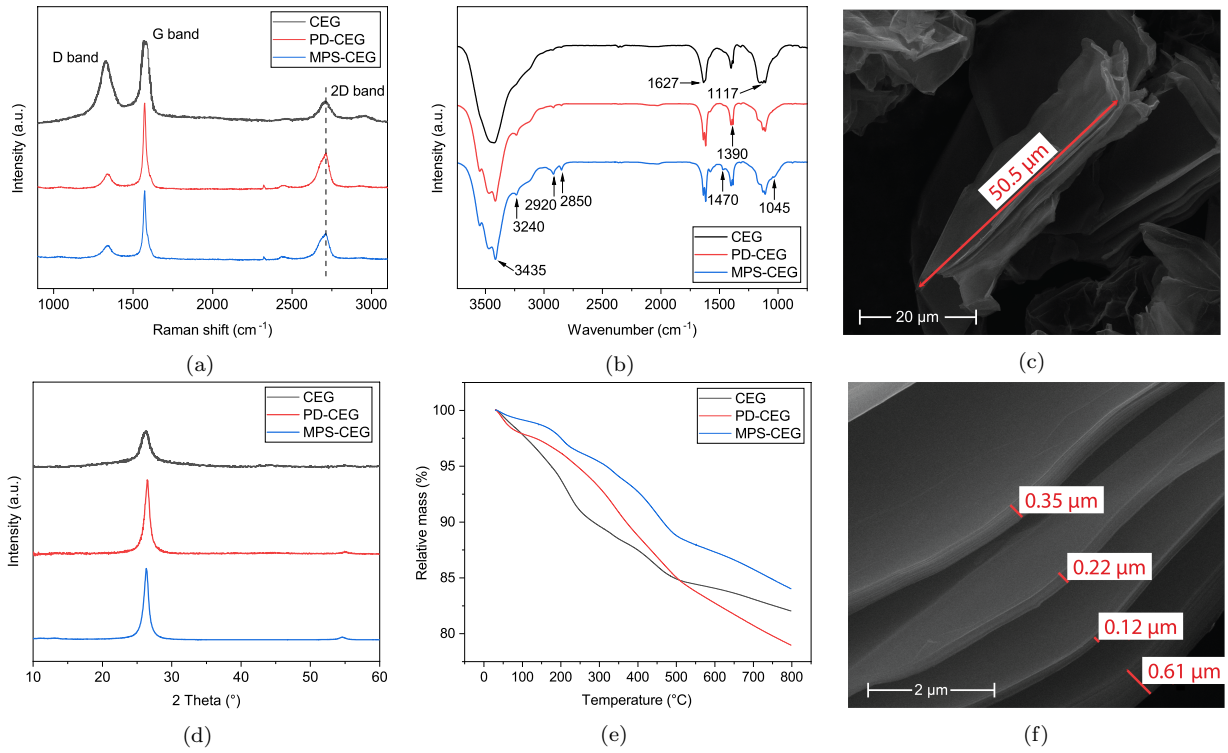

Figure 2: Characterisation results of CEG and f-CEG a) Raman spectrum, b) FTIR infrared spectrum, c) SEM micrograph of CEG, d) XRD diffraction pattern, e) TGA mass loss curves and f) SEM micrograph of CEG indicating the sheet thickness

The spectra obtained by Raman spectroscopy, presented in figure 2a, showed a large reduction in relative D-band intensity for the functionalized CEG. The I_D/I_G ratio, as determined by maximum peak intensity, was 0.76 for the CEG and reduced to 0.20 and 0.23 for PD-CEG and MPS-CEG, respectively. The change in I_D/I_G ratio indicates a restoration of the SP^2 domain which could be due to the reduction of CEG [26]. The three FTIR spectra of the functionalized and non-functionalized CEG can be found in figure 2b. The FTIR spectrum for the pure CEG shows clear graphitic features with a peak at 1627 cm $^{-1}$ due C=C stretching. The vibration of -OH groups appears as an intense broad peak at 3435 cm^{-1} including some smaller peaks such as the one found at 3240 cm^{-1}. At both 1390 cm $^{-1}$ and 1117 cm^{-1} peaks were identified related to -CO stretching vibrations, indicating the presence of oxygen moieties on the CEG surface. For PD-CEG, no new peaks could be identified by FTIR which can likely be attributed to a low degree of functionalization or peak

overlap with the main CEG peaks. For the MPS-functionalized CEG, a higher peak intensity at 2850 cm^{-1} and 2920 cm^{-1} was present due to the symmetric and asymmetric vibrations of the alkyl groups of the MPS molecules. Two small peaks appeared at 740 cm^{-1} and 1470 cm^{-1} which can also be ascribed to -CH_2 bonds. Furthermore, at 1045 cm^{-1} a minor increase in peak intensity was found which can be related to stretching of Si-O-C bonds by MPS functionalization [27].

The full XPS spectra of CEG and f-CEG are presented in figure 3. Deconvolution of the carbon 1S peak of CEG (see figure 3d) shows two contributions at 284.6 eV and 286 eV, which correspond C-C bonding of the SP^2 hybridized carbon and C-O bonding, respectively. The contribution of C-O bonds was used to determine an oxygen content of 14.4%. The O1s peak shows the presence of mainly hydroxyl and epoxy groups. A notable quantity of sulphur was furthermore found, likely corresponding to remaining sulphuric acid from forming the GIC. For PD-CEG, the nitrogen peak showed two contributions at 399.9 eV and 401.9 eV (see figure 3e) related to amine and protonated amine, respectively [28]. The protonated amine peak corresponds to the presence of dopamine whereas the amine peak can be assigned to the presence of polydopamine, indicating both functionalization and polymarization. Assuming a single amine group per polydopamine molecule, the total contribution of the nitrogen amine peaks allowed for a degree of functionalization of 1.03 at%. For MPS-CEG, at 102.5 eV a new peak was observed related to the Si 2p peak, see figure 3f, which be assigned to MPS molecules. The degree of functionalization could be estimated to be 0.15 at%. For both functionalised CEG species, the oxygen content reduced significantly. PD-CEG and MPS-CEG had an oxygen content of 7.7% and 8.6%, respectively. The self-polymerization reaction of dopamine to form polydopamine is known to reduce graphene oxide [29]. For silane compounds, the condensation reaction takes away the hydroxyl groups by forming N-H bonds, reducing the oxygen content[30]. Alternatively, the consistent reduction for both functionalized species could be related to solvothermal reduction. At high temperatures, alcohols, including ethanol, have shown to be effective media to reduce graphite oxide [31, 32]. The reduced C-O peak in the carbon 1S spectrum indicates the removal of mainly epoxy and hydroxyl groups, which are expected to be removed at the lowest temperatures [33].

XRD of the CEG provided a broad 002 diffraction beak at 26.4°, see figure 2d. This peak corresponds to that of unexpanded graphite. The weak intensity and wide nature are related to the oxidation of the starting graphite [27]. Both the PD and MPS-CEG showed increases in peak intensity which has previously also been found by wang et al. for MPS decorated CEG [22]. Likely the reduction of CEG by the functionalization process allows for the partial restoration of the initial graphitic lamellar structure, giving rise to an enhanced 002 peak intensity. The mass loss curves as found by TGA can be found in figure 2e. The mass loss of the pure CEG indicated an oxygen content of 15 wt%, closely matching the XPS data. Although TGA is considered a powerful tool to determine the degree of functionalization, the evident reduction of CEG makes determining the degree of functionalization challenging. The curves for PD-CEG and MPS-CEG do however clearly indicate the successful functionalization by introducing new degradation mechanisms of the organic functionalization compounds.

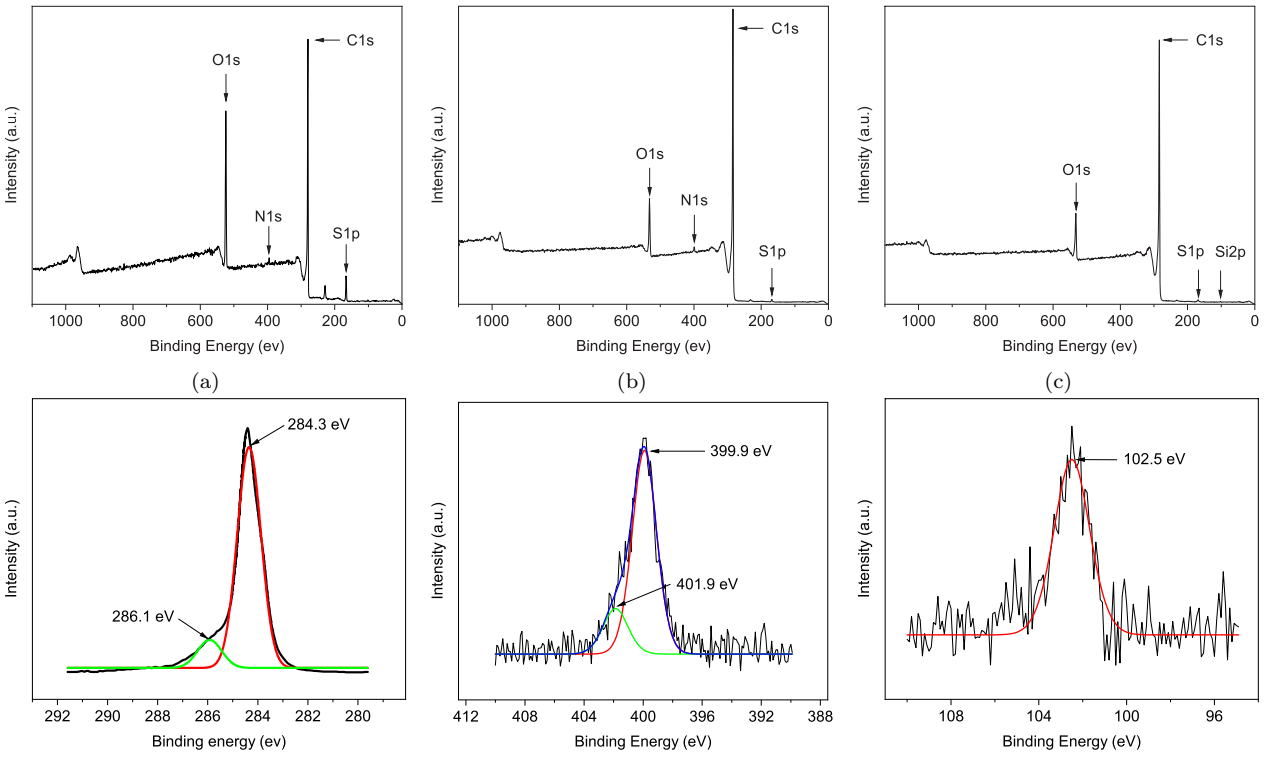

Figure 3: The full XPS spectra and relevant XPS peaks of: a,d) CEG, b,e) PD-CEG and c,f) MPS-CEG

3.2. Optical characterisation

SEM micrographs of the obtained CEG can be found in figures 2c and 2f. A reduction in average sheet size from 300+ µm to 50 µm can clearly be observed following the synthesis of CEG by oxidation and expansion. Sheet stacks with a thickness from 0.12 µm up to 0.61 µm were measured prior to exfoliation. The 5 wt% composite powder morphology prior to consolidation can be found in figure 4. When compared to CEG, MPS-CEG appears in larger and thicker aggregations. This is likely due to the inability of MPS-CEG to exfoliate and disperse efficiently in the highly polar ethanol. For PD-CEG an enhancement in exfoliation is visible with thinner and more wrinkled aggregations and a higher coverage of the polymer powder. These observations are in line with the disperability studies of CEG and f-CEG in both ethanol and NMP which are presented in figure S1. The enhanced exfoliation and dispersion of PD-CEG can be explained by the polar nature of ethanol which has a better affinity towards the PD terminations. By drop casting ethanol dispersion on aluminium sem stubs, the degree of exfoliation was furthermore studied. The SEM micrographs are presented in figure S2.

High magnification images of the fracture surfaces of the pure polymer and 1 wt% composites are presented in figure 5. The pure polymer fracture surface appears rather uniform with clear features of a ductile fracture. For the non-modified CEG, aggregates of CEG were identified without a sign of a good interfacial bonding with the matrix and clear pull-out gaps on the surface. This is an indication that the lamellar structure is largely maintained without efficient exfoliation. The PD functionalization had a significant effect on the exfoliation as thinner sheets were clearly visible and more properly distributed throughout the polymer (figure 5c). However, no signs of an enhanced interface with the polymer were identified. In contrast, the MPS modified CEG demonstrated a stronger adhesion to the polymer with chains covering sheets of the f-CEG at the fracture surface, as highlighted in figure 5d. Furthermore, the surrounding polymer showed more plastic deformation indicating a more ductile fracture. However, non-bonded MPS-CEG surfaces were still visible, which relate to aggregates and their weak interplanar bonding. Similar features were identified for all tested concentrations.

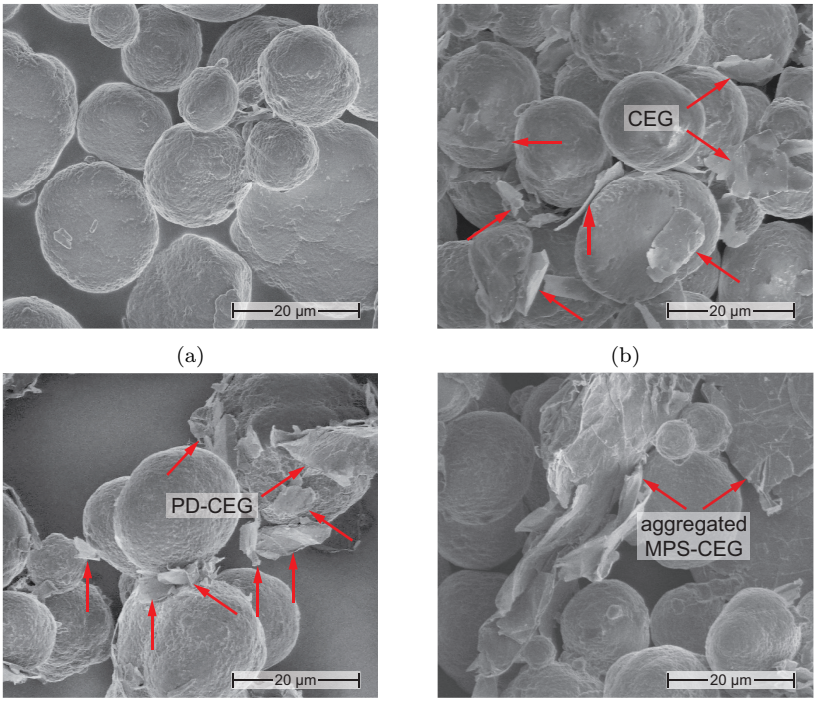

Figure 4: SEM micrographs of powder morphology of: a) UHMWPE, b) 5 wt% CEG, c) 5 wt% PD-CEG, d) 5 wt% MPS-CEG The red arrows indicate the CEG and f-CEG sheets along the polymer particles

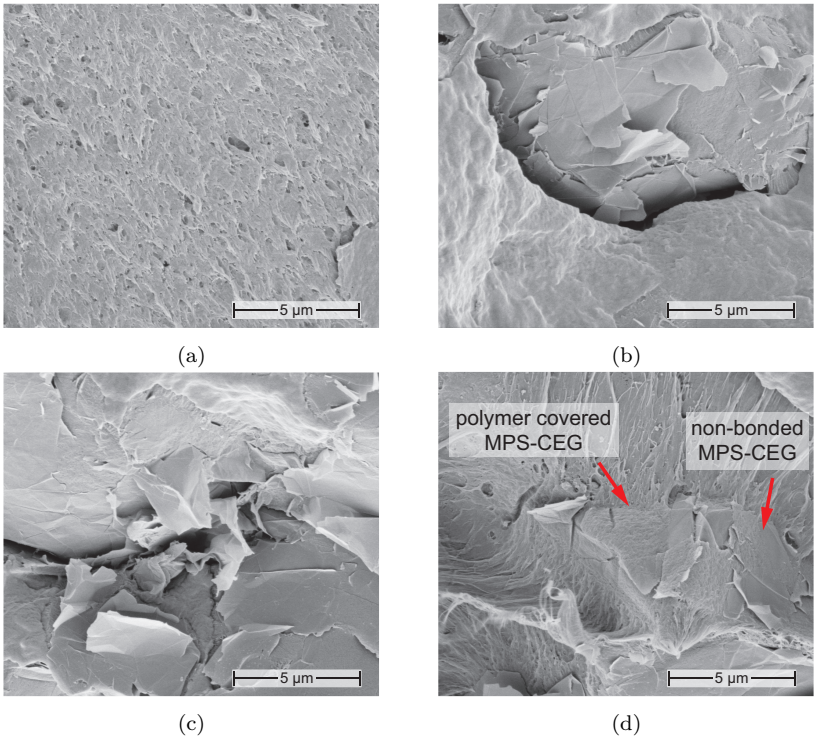

Figure 5: SEM micrographs of the fracture surfaces from: a) UHMWPE b) 1% CEG c) 1% PD-CEG d) 1% MPS-CEG

3.3. DSC

The obtained degrees of crystallinity for the composites can be found in figure 6a. For PD-CEG, a reduction in degree of crystallinity was obtained for all tested concentrations. With respect to CEG and MPS-CEG, PD-CEG provided a clearly enhanced dispersion which enhances the reinforcement's ability to obstruct crystallisation by obstructing the polymer chain mobility and fusing of the UHMWPE powder. For both the CEG and MPS-CEG composites no statistically significant differences were found. The average peak melting temperatures for the different composites can be found in figure 6b and the melting curves are provided in figure S3. All composites clearly have a reduced melting temperature with respect to the pure polymer. By obstructing the chain mobility and thereby the fusing of individual powder particles crystallites with a lower lamella thickness are formed. Identical behaviour has previously been identified by Wu et al. for boron nitride UHMWPE composites [34]. For GO based composites previously obtained results indicated no clear change in melting temperature [35, 36]. The obtained reduction in melting temperature could also be attributed the enhanced thermal conductivity due to the introduction of CEG. Similar to the work by Wu et al. the high thermal conductivity of the reinforcement could enable the temperature to reach the bulk at a higher rate, advancing the obtained peak melting temperature upon heating. For GO, the higher degree of oxidation could suppress this effect by significantly reducing the thermal conductivity [37].

3.4. Mechanical characterisation

The DMA results, as presented in figure 7, show the storage and loss moduli with respect to temperature as obtained under 10 Hz. The storage modulus, G', represents the elastic component of the viscoelasticity whereas the loss modulus, G", represents the energy which is dissipated and thereby denotes the viscous portion. The storage modulus at room temperature decreases by 14% from 737.2 MPa to 630.9 MPa when introducing 1 wt% CEG with respect to pure UHMWPE. The initial decrease in storage modulus has previously also been found for expanded graphite and graphite oxide by Rocha et al. at a reinforcement content of 0.5 wt% [38]. An identical decrease was also observed for lower percentages of rGO in polyethylene [39, 40, 41]. Pang et al. showed an increase in storage modulus of 13% for 0.5

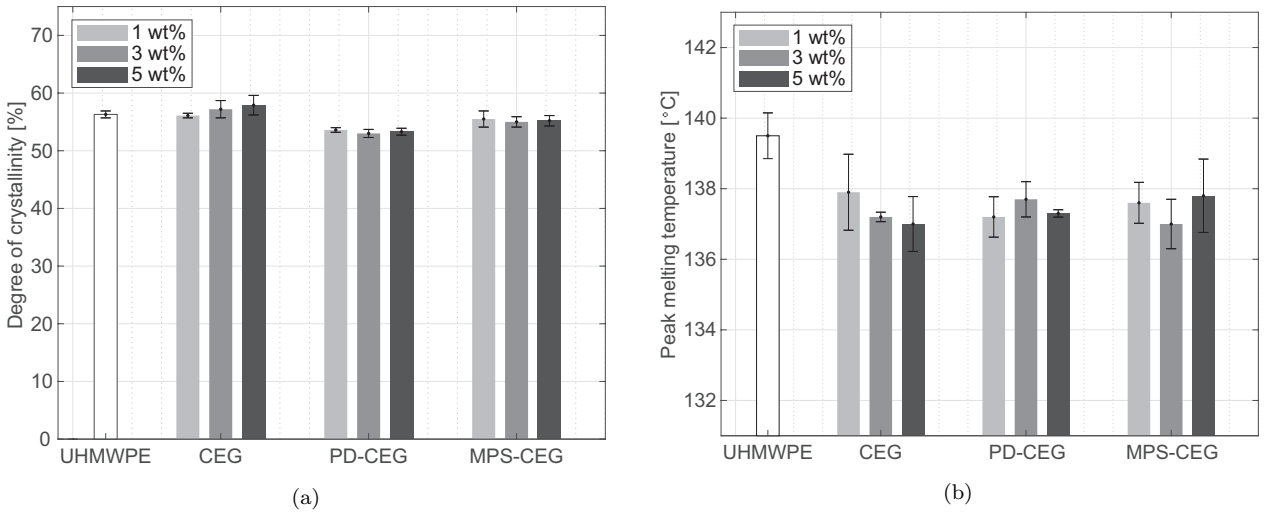

Figure 6: DSC results of UHMWPE and composite materials showing the a) degree of crystallinity and b) peak melting temperature

wt% GO in UHMWPE. However, when increasing the GO content from 0.5 to 1 wt%, the storage modulus decreased significantly, obtaining a value lower than for pure UHMWPE [42]. Interestingly, a similar but more severe decrease (36% reduction) was present for 1 wt% MPS-CEG. PD-CEG, in contrast, provided a slight increase (5%) in storage modulus with respect to the pure polymer. The decrease in room temperature storage modulus for both 1 wt% CEG and MPS-CEG is likely related to their poor dispersion as described previously. At a low content the presence of aggregates, which were identified by SEM, obstructs the effective stress transfer between UHMWPE particles. At higher concentrations of 3 and 5 wt%, the reinforcement effect is enhanced, increasing G' with 13% and 15% when compared to UHMWPE, respectively. For 5 wt% MPS-CEG, a storage modulus of 979.7 MPa was obtained, an increase of 32%. For PD-CEG, all tested percentages provided an enhanced storage modulus with a maximum increase at 5 wt% to 992.3 MPa, providing a 34% increase in storage modulus with respect to UHMWPE. These improvements are in the same range as obtained for 5wt% rGO, graphite and expanded graphite based polyethylene composites prepared using melt mixing techniques, see table 1. In comparison to these results, the use of functionalized CEG introduces a simple and scalable approach to prepare high performance graphene based polymer composites. The authors suggest the use of melt mixing to further enhance the exfoliation and dispersion of CEG which could amplify the improvements in mechanical properties [22].

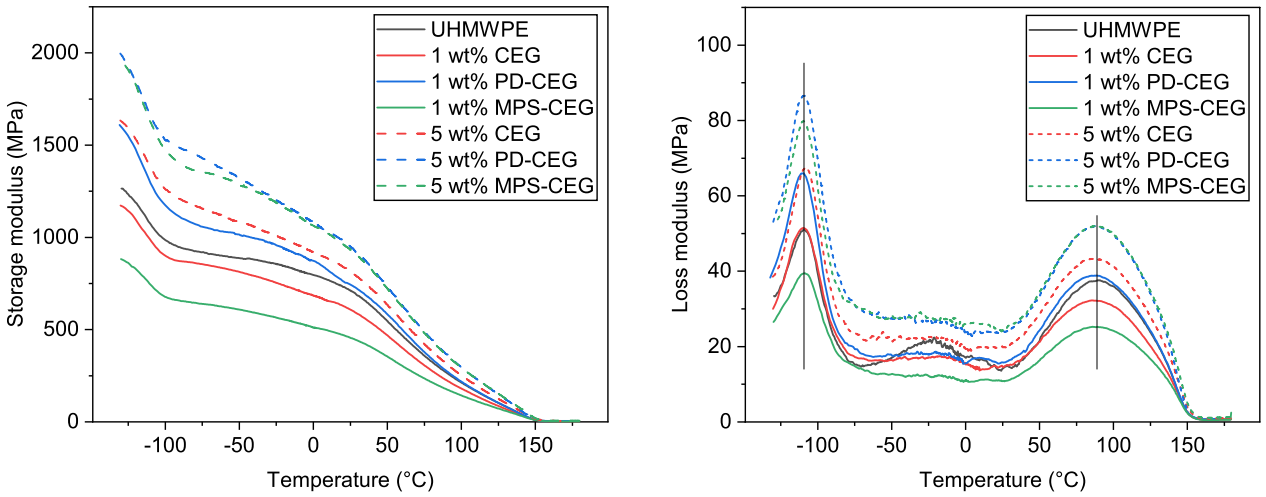

(a) (b)

Figure 7: ()a) Storage and b) loss modulus curves of UHMWPE and composites with a reinforcement content of 1 wt% and 5 wt% at 10 Hz

Material	Filler content	G' improvement	Ref.
HDPE/rGO	5 wt%	33%	[47]
HDPE/expanded graphite	5 wt%	∼50%	[48]
HDPE/expanded graphite	5 wt%	34%	[45]
UHMWPE/CEG	5 wt%	7%	[11]
UHMWPE/CEG	5 wt%	15%	This work
UHMWPE/PD-CEG	5 wt%	34%	This work
UHMWPE/MPS-CEG	5 wt%	32%	This work

Table 1: Relative improvement in storage modulus with respect to the pure matrix at room temperature

The relative and absolute enhancements in storage modulus by introducing the CEG decreases at increasing temperatures. The maximum enhancements as obtained at -100°C were 28%, 50%, 58% for 5 wt% CEG, PD-CEG and MPS-CEG, respectively, highlighting the potential of these composites for use at low temperature applications. Similar behavior has previously also been found for multiwalled carbon nanotube / epoxy composites by Chen et al. under cryogenic temperatures, the authors found a more pronounced reinforcement due to the large differences in thermal expansion coefficient causing the polymer to shrink around the reinforcement, enhancing the interface strength between the matrix and MWCNTs [49]. It is likely that the obtained results by introducing CEG and f-CEG rely on the same mechanism.

The loss moduli, as presented in figure 7b, show two main relaxation mechanisms appearing as peaks. The γ relaxation at around -120°C is related to the chain motion in the amorphous phase and indicates the glass transition. The α relaxation relates to chain motion within the crystalline phase. No clear differences in glass transition temperature were obtained. This could be an indication that the amorphous phase of the polymer is unaffected by the introduction of the reinforcements. However, with the heating rate being a factor 5 lower than what was used in DSC experiments, the thermal gradient in the sample is also reduced. This negates the influence of thermal conductivity on the measured thermal transition temperatures which could alternatively explain the absence of differences in T_g for the pure polymer and the composites.

The reinforcement efficiency factor, r, as presented in table 2 shows that CEG and f-CEG are most efficient at 3 wt%. Increasing the reinforcement content does enhance the storage modulus but due to a higher amount of aggregates, a higher content is increasingly less efficient. The adhesion factors for the different materials are presented in table 2. For well dispersible reinforcements, an enhanced interfacial adhesion reduces the chain mobility of the matrix close to the reinforcement. This reduces the damping of the matrix, lowering the $tan\ \delta$ and adhesion factor. The limit of adhesion is $A = 0$, where lower A-factors indicate interfacial adhesion [50]. The values in table 2 are high when compared to literature [50, 25]. When comparing the CEG with f-CEG, MPS-CEG provides a higher adhesion factor than CEG whereas PD-CEG has the lowest adhesion factor at a concentration of 1 wt%. For all reinforcements, the highest concentration of 5 wt% also provided the highest adhesion factor. While the model assumes no damping by the reinforcement, the results indicate that the damping is increased for MPS-CEG and higher concentrations of all reinforcements. This increase is likely not due to the interface adhesion itself but damping by the multilayer CEG, which dissipates energy through internal friction of the layers [51]. A high concentration of CEG/f-CEG in the composite, prevents an adequate dispersion, enhancing the content of aggregates and therefore the damping. Similar results have in the past been obtained for graphite based composites [52].

Sample	G' [MPa]	G" [MPa]	r	A	Micro-hardness [HV]
UHMWPE	737.2	12.5	-	-	4.24 ± 0.07
1 wt% CEG	630.9	14.5	-14.4	0.20	4.10 ± 0.08
3 wt% CEG	831.6	17.4	4.4	0.13	4.14 ± 0.05
5 wt% CEG	851.2	19.9	3.0	0.28	4.16 ± 0.05
1 wt% PD-CEG	773.4	11.2	4.4	0.10	4.33 ± 0.09
3 wt% PD-CEG	939.8	22.0	9.2	0.11	5.06 ± 0.09
5 wt% PD-CEG	992.3	24.6	6.7	0.25	5.10 ± 0.14
1 wt% MPS-CEG	474.9	15.6	-35.8	0.39	4.30 ± 0.05
3 wt% MPS-CEG	960.9	21.6	9.8	0.23	5.31 ± 0.15
5 wt% MPS-CEG	979.7	23.5	6.3	0.23	4.94 ± 0.14

Table 2: DMA and micro hardness data at 23°C

The micro hardness values can be found in table 2. The addition of CEG induces a slight reduction in micro hardness from 4.24 to 4.10 HV although increasing when introducing a higher content. These results are in line with the above presented DMA results. Both species of surface functionalised CEG increase the micro hardness, especially for a higher content of 3 wt% and 5 wt%. For MPS-CEG, a maximum micro hardness of 5.31 HV was obtained at 3 wt%, whereas a value of 5.10 HV was obtained using 5 wt% PD-CEG, respective increases of 25% and 20%. The higher hardness for f-CEG can be explained by two mechanisms. For the PD-CEG an enhanced exfoliation was present, increasing the available surface area to transfer stress from the polymer with respect to the aggregated non-functionalized CEG. For the MPS-functionalization, the previously discussed indications of an enhanced interface with the polymer explain the prevailing increase in hardness as obtained at 3 wt% and 5 wt%.

3.5. Wettability and wear characterisation

The low wettability of UHMWPE is an important characteristic for the low friction and wear performance of the polymer in lubricated contacts [54]. The surface wettability to water as determined by the contact angles can be found in figure 8a. The results clearly show the effect of the low degree of oxidation of CEG. The water contact angle increases with respect to pure UHMWPE (98.6°) as a function of the CEG content with the 5 wt% CEG providing the most hydrophobic surface with a contact angle of 107.2°. These values are significantly

higher than the results obtained for GO / UHMWPE composites [35] and in the same range as the contact angle found for recent work on onion like carbon / UHMWPE composite [55]. The effect of functionalization with PD and MPS is furthermore clearly visible at high CEG contents. MPS increases the water contact angle as is often found for this compound [24]. The highest contact angle for MPS-CEG was found for 5 wt%, providing a contact angle of 119.0°. Polydopamine functionalization with the presence of hydroxyl groups does not provide the same degree of increase in water contact angle.

The surface free energy (SFE) follows the same trend as obtained for the water contact angle (see figure 8b) with a lower SFE when increasing the CEG and MPS-CEG content. Noteworthy is the trend for PD-CEG which provides an increase in SFE at an increasing content. This likely is a result of the surface chemistry but also an enhanced exfoliation allowing for more PD-CEG to cover the specimen surface. Although the surface roughness parameters were identical for all samples, the surface roughness along with the local surface chemistry could play a dominant factor in surface wettability. The results from the preliminary tribological experiments are presented in figure 9. The results show that for 5 wt% MPS-CEG, the wear rate was reduced by 99%, which is notably higher than the reduction obtained using GO or rGO [56, 57]. For the 5 wt% CEG, this reduction was less significant at 83%. The difference can be explained by the enhanced mechanical properties through the interface adhesion between the MPS-CEG and the polymer along with the increased hydrophobicity which enables more effective lubrication of distilled water. The higher wear at 5 wt% for CEG and PD-CEG when compared to 1 wt% can be explained by the higher content of aggregates which can act as defects in the composite and thereby promoting wear.

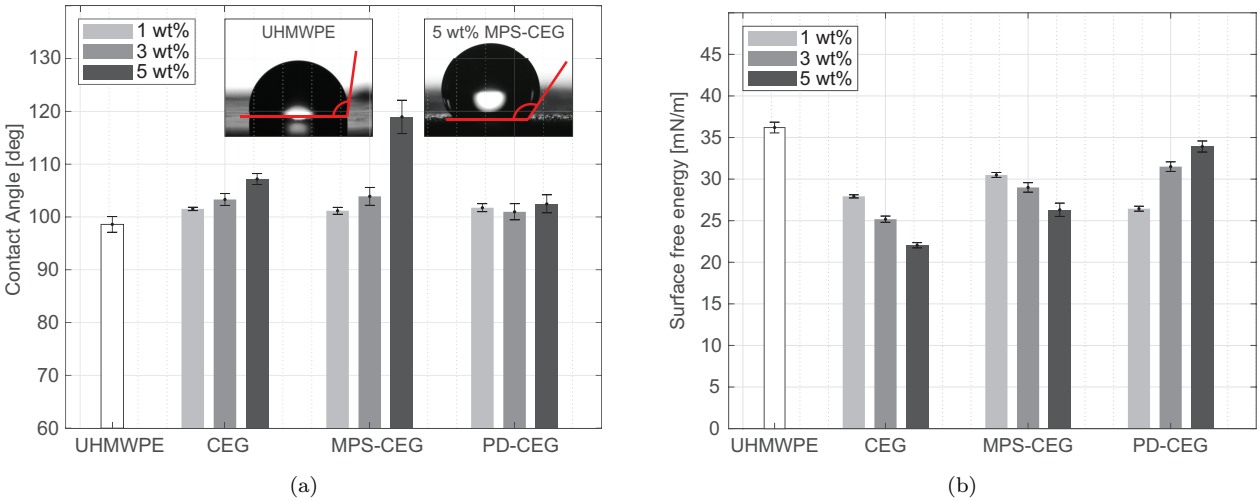

Figure 8: Surface wettability of UHMWPE and composite materials as indicated by the: a) water contact angle and b) surface free energy

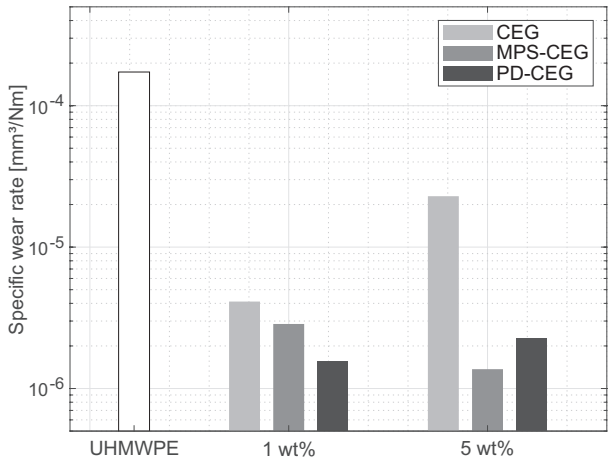

Figure 9: Preliminary specific wear rates from the tribological experiments

4. Conclusions

CEG was successfully prepared with oxygen values closely resembling values found in literature. MPS and PD molecules were furthermore successfully grafted onto the CEG. XPS analyses indicated a reduction in oxygen content by functionalization preventing the efficient exfoliation of CEG in ethanol and thereby reducing the obtainable degree of functionalization. PD functionalized CEG, provided an enhanced dispersability in the polymer matrix with respect to the non-modified CEG. Additionally the MPS-functionalization enhanced the interface with the polymer as was visible from fracture surfaces. At higher reinforcement

contents of 3 wt% and 5 wt%, the mechanical properties were significantly enhanced for CEG and both functionalized CEG species, especially at low temperatures with an increase in storage modulus of up to 58% by 5 wt% PD-CEG. The wettability was furthermore reduced upon addition of CEG and MPS-CEG with particularly high water contact angles for the MPS-CEG composites, making the material highly hydrophobic. Under water lubricated conditions, the composites had an enhanced wear resistance during the preliminary tribological evaluation with a decrease in wear of up to 99%. CEG and especially functionalized CEG proved to be promising reinforcements for use in polymer composites with the ability for commercial up-scaling. The enhanced mechanical properties, along with the wettability and wear resistance, indicate the potential of the composites for use in tribological applications.

5. Acknowledgements

The authors would like to acknowledge the support from M. Larsson by performing the Raman measurements. The research is financially supported by Vinnova as part of the SIO Grafen programme (reference number: 2017-03609). G.G. gratefully acknowledges the Portuguese Science Foundation (FCT) for Programme Stimulus of Scientific Employment—Individual Support (CEECIND/01913/2017) and financial support of TEMA by the projects UIDB/00481/2020 and UIDP/00481/2020; and CENTRO-01-0145-FEDER-022083—Centro Portugal Regional Operational Programme (Centro 2020), under the PORTUGAL 2020 Partnership Agreement, through the European Regional Development Fund. Finally, the authors would like to acknowledge the financial support via the 3D - PRINTGRAPH project (Grant agreement ID: 705875).

References

[1] M. Tabish, M. U. Malik, M. A. Khan, G. Yasin, H. M. Asif, M. J. Anjum, W. Q. Khan, S. Ibraheem, T. A. Nguyen, Y. Slimani, M. T. Nazir, Construction of nico/graphene nanocomposite coating with bulges-like morphology for enhanced mechanical properties and corrosion resistance performance, Journal of Alloys and Compounds 867 (2021) 159138. doi:10.1016/j.jallcom.2021.159138.

[2] A. Kumar, K. Sharma, A. Dixit, A review on the mechanical properties of polymer composites reinforced by carbon nanotubes and graphene, Carbon Letters 31 (2020) 149–165. doi:10.1007/s42823-020-00161-x.

[3] T. Ramanathan, A. A. Abdala, S. Stankovich, D. A. Dikin, M. Herrera-Alonso, R. D. Piner, D. H. Adamson, H. C. Schniepp, X. Chen, R. S. Ruoff, S. T. Nguyen, I. A. Aksay, R. K. Prud'Homme, L. C. Brinson, Functionalized graphene sheets for polymer nanocomposites, Nature Nanotechnology 3 (2008) 327–331. doi:10.1038/nnano.2008.96.

[4] L. Melk, N. Emami, Mechanical and thermal performances of uhmwpe blended vitamin e reinforced carbon nanoparticle composites, Composites Part B: Engineering 146 (2018) 20–27. doi:10.1016/j.compositesb.2018.03.034.

[5] P. Mukhopadhyay, R. K. Gupta, Graphite, Graphene, and their polymer nanocomposites, CRC press, 2012.

[6] C. Wan, B. Chen, Reinforcement and interphase of polymer/graphene oxide nanocomposites, Journal of Materials Chemistry 22 (2012) 3637–3646. doi:10.1039/C2JM15062J.

[7] Y. Fu, J. Zhang, H. Liu, W. C. Hiscox, Y. Gu, Ionic liquid-assisted exfoliation of graphite oxide for simultaneous reduction and functionalization to graphenes with improved properties, Journal of Materials Chemistry A 1 (2013) 2663–2674. doi:10.1039/c2ta00353h.

[8] X. Yang, T. Mei, J. Yang, C. Zhang, M. Lv, X. Wang, Synthesis and characterization of alkylamine-functionalized graphene for polyolefin-based nanocomposites, Applied Surface Science 305 (2014) 725–731. doi:10.1016/j.apsusc.2014.03.184.

[9] S. Lin, L. Dong, J. Zhang, H. Lu, Room-temperature intercalation and 1000-fold chemical expansion for scalable preparation of high-quality graphene, Chemistry of Materials 28 (2016) 2138–2146. doi:10.1021/acs.chemmater.5b05043.

[10] P. Wang, M. Li, J. Zhang, L. Dong, H. Lu, High-yield water-phase exfoliated few-defect graphene for high performance polymer nanocomposites, Journal of Applied Polymer Science 137 (2020). doi:10.1002/app.49586.

[11] V. de Oliveira Aguiar, V. J. Roget Rodriguez Pita, M. de Fatima Vieira Marques, I. T. Soares, E. H. Martins Ferreira, M. S. Oliveira, S. N. Monteiro, Ultra-high molecular weight polyethylene nanocomposites reinforced with novel surface chemically modified sonic-exfoliated graphene, Journal of Materials Research and Technology 11 (2021) 1932–1941. doi:10.1016/j.jmrt.2021.02.027.

[12] N. Saravanan, R. Rajasekar, S. Mahalakshmi, T. P. Sathishkumar, K. S. K. Sasikumar, S. Sahoo, Graphene and modified graphene-based polymer nanocomposites – a review, Journal of Reinforced Plastics and Composites 33 (2014) 1158–1170. doi:10.1177/0731684414524847.

[13] L. Q. Xu, W. J. Yang, K. G. Neoh, E. T. Kang, G. D. Fu, Dopamine-induced reduction and functionalization of graphene oxide nanosheets, Macromolecules 43 (2010) 8336–8339. doi:10.1021/ma101526k.

[14] Q. Wu, X. Yang, Z. Ye, H. Deng, J. Zhu, Dopamine-dependent graphene oxide modification and its effects on interfacial adhesion of carbon fiber composites, Surfaces and Interfaces 31 (2022) 102086. doi:10.1016/j.surfin.2022.102086.

[15] N. Huang, S. Zhang, L. Yang, M. Liu, Y. Zhang, S. Yao, Multifunctional electrochemical platforms based on the michael addition/schiff base reaction of polydopamine modified reduced graphene oxide: Construction and application, ACS applied materials & interfaces 7 (2015). doi:10.1021/acsami.5b04597.

[16] L. A. Burzio, J. H. Waite, Cross-linking in adhesive quinoproteins: Studies with model decapeptides, Biochemistry 39 (2000) 11147–11153. doi:10.1021/bi0002434.

[17] Y. Fu, L. Liu, J. Zhang, W. C. Hiscox, Functionalized graphenes with polymer toughener as novel interface modifier for property-tailored polylactic acid/graphene nanocomposites, Polymer 55 (2014) 6381–6389. doi:10.1016/j.polymer.2014.10.014.

[18] Y. J. Wan, L. X. Gong, L. C. Tang, L. B. Wu, J. X. Jiang, Mechanical properties of epoxy composites filled with silane-functionalized graphene oxide, Composites Part A: Applied Science and Manufacturing 64 (2014) 79–89. doi:10.1016/j.compositesa.2014.04.023.

[19] N. I. Khan, S. Halder, S. Das, J. Wang, Exfoliation level of aggregated graphitic nanoplatelets by oxidation followed by silanization on controlling mechanical and nanomechanical performance of hybrid cfrp composites, Composites Part B: Engineering 173 (2019) 106855. doi:10.1016/j.compositesb.2019.05.066.

[20] C. Velasco-santon, A. Martinez-hernandez, M. Lozada-Cassou, A. Alvarez-Castilla, V. Casano, Chemical functionalization of carbon nanotubes through an organosilane, Nanotechnology 13 (2002) 495–498. doi:10.1088/0957-4484/13/4/311.

[21] P. C. Ma, J.-k. Kim, B. Z. Tang, Functionalization of carbon nanotubes using a silane coupling agent, Carbon 44 (2006) 3232–3238. doi:10.1016/j.carbon.2006.06.032.

[22] P. Wang, J. Zhang, L. Dong, C. Sun, X. Zhao, Y. Ruan, H. Lu, Interlayer polymerization in chemically expanded graphite for preparation of highly conductive, mechanically strong polymer composites, Chemistry of Materials 29 (2017) 3412–3422. doi:10.1021/acs.chemmater.6b04734.

[23] P. Wang, H. Chong, J. Zhang, Y. Yang, H. Lu, Ultralow electrical percolation in melt-compounded polymer composites based on chemically expanded graphite, Composites Science and Technology 158 (2018) 147–155. doi:10.1016/j.compscitech.2018.01.022.

[24] R. Yuan, P. Ju, Y. Wu, L. Ji, H. Li, L. Chen, Silane-grafted graphene oxide improves wear and corrosion resistance of polyimide matrix : molecular dynamics simulation and experimental analysis, Journal of Materials Science 54 (2019) 11069–11083. doi:10.1007/s10853-019-03672-9.

[25] C. Correa, C. Razzino, J. E. Hage, Role of maleated coupling agents on the interface adhesion of polypropylene—wood composites, Journal of Thermoplastic Composite Materials 20 (2007) 323–339. doi:10.1177/0892705707078896.

[26] G. Yasin, M. J. Anjum, M. U. Malik, M. A. Khan, W. Q. Khan, M. Arif, T. Mehtab, T. A. Nguyen, Y. Slimani, M. Tabish, D. Ali, Y. Zuo, Revealing the erosion-corrosion

performance of sphere-shaped morphology of nickel matrix nanocomposite strengthened with reduced graphene oxide nanoplatelets, Diamond and Related Materials 104 (2020) 107763. doi:10.1016/j.diamond.2020.107763.

[27] Y. Lin, J. Jin, M. Song, Preparation and characterisation of covalent polymer functionalized graphene oxide, Journal of Materials Chemistry 21 (2011) 3455–3461. doi:10.1039/c0jm01859g.

[28] T. Liu, K. C. Kim, B. Lee, Z. Chen, S. Noda, S. S. Jang, S. W. Lee, Self-polymerized dopamine as an organic cathode for li- and na-ion batteries, Energy Environ. Sci. 10 (2017) 205–215. doi:10.1039/C6EE02641A.

[29] X. Zhao, J. Pionteck, Electrochemical performance of polydopamine modified pani/rgo composites: Dependency on preparation sequence, Journal of Applied Polymer Science 138 (2021) 50663. doi:10.1002/app.50663.

[30] Y. J. Kim, H. C. Park, B. K. Kim, Triple shape-memory effect by silanized graphene oxide nanocomposites bilayer, High Performance Polymers 27 (2015) 886–897. doi:10.1177/0954008314565398.

[31] D. R. Dreyer, S. Murali, Y. Zhu, R. S. Ruoff, C. W. Bielawski, Reduction of graphite oxide using alcohols, Journal of Materials Chemistry 21 (2011) 3443–3447. doi:10.1039/c0jm02704a.

[32] C. Paiva, P. Soares, R. D. L. Baptista, D. V. Cesar, Solvothermal reduction of graphite oxide using alcohols, Materials Research 21 (2018) 1–7. doi:10.1590/1980-5373-mr-2017-0726.

[33] S. Mao, H. Pu, J. Chen, Graphene oxide and its reduction: Modeling and experimental progress, RSC Advances 2 (2012) 2643–2662. doi:10.1039/c2ra00663d.

[34] X. Wu, W. Liu, L. Ren, C. Zhang, Highly thermally conductive boron nitride-uhmwpe composites with segregated structure, e-Polymers 20 (2020) 510–518. doi:10.1515/epoly-2020-0053.

[35] S. Suñer, R. Joffe, J. Tipper, N. Emami, Ultra high molecular weight polyethylene/graphene oxide nanocomposites: Thermal, mechanical and wettability characterisation, Composites Part B: Engineering 78 (2015) 185–191. doi:10.1016/j.compositesb.2015.03.075.

[36] L. P. Belotti, H. S. Vadivel, N. Emami, Tribological performance of hygrothermally aged uhmwpe hybrid composites, Tribology International 138 (2019) 150–156. doi:10.1016/j.triboint.2019.05.034.

[37] X. Mu, X. Wu, T. Zhang, D. Go, T. Luo, Thermal transport in graphene oxide – from ballistic extreme to amorphous limit, Scientific reports 4 (2014) 3909. doi:10.1038/srep03909.

[38] L. Felipe M. Rocha, S. B. Cordeiro, L. C. Ferreira, F. James H. Ramos, M. de Fátima Marques, Effect of carbon fillers in ultrahigh molecular weight polyethylene matrix prepared by twin-screw extrusion, Journal of Materials Sciences and Applications 7 (2016) 863–880. doi:10.4236/msa.2016.712066.

[39] Z. Seibers, M. Orr, G. S. Collier, A. Henriquez, M. Gabel, M. L. Shofner, V. La Saponara, J. Reynolds, Chemically functionalized reduced graphene oxide as additives in polyethylene composites for space applications, Polymer Engineering & Science 60 (2020) 86–94. doi:10.1002/pen.25262.

[40] K. Liu, S. Ronca, E. Andablo-Reyes, G. Forte, S. Rastogi, Unique rheological response of ultrahigh molecular weight polyethylenes in the presence of reduced graphene oxide, Macromolecules 48 (2015) 131–139. doi:10.1021/ma501729y.

[41] T. McNally, P. Pötschke, P. Halley, M. Murphy, D. Martin, S. E. Bell, G. P. Brennan, D. Bein, P. Lemoine, J. P. Quinn, Polyethylene multiwalled carbon nanotube composites, Polymer 46 (2005) 8222–8232. doi:10.1016/j.polymer.2005.06.094, controlled Macromolecular Synthesis and Controlled Architectures - Supramolecular Polymer Assemblies.

[42] W. Pang, Z. Ni, G. Chen, G. Huang, H. Huang, Y. Zhao, Mechanical and thermal properties of graphene oxide/ultrahigh molecular weight polyethylene nanocomposites, RSC Adv. 5 (2015) 63063–63072. doi:10.1039/C5RA11826C.

[43] T. Dayyoub, A. V. Maksimkin, S. Kaloshkin, E. Kolesnikov, D. Chukov, T. P. Dyachkova, I. Gutnik, The structure and mechanical properties of the uhmwpe films modified by the mixture of graphene nanoplates with polyaniline, Polymers 11 (2019). doi:10.3390/polym11010023.

[44] I. Tavman, I. Krupa, M. Omastova, M. Sarikanat, I. Novak, K. Sever, I. Ozdemir, Y. Seki, S. Podhradská, D. Moskova, E. Erbay, F. Guner, Effects of conductive graphite filler loading on physical properties of high-density polyethylene composite, Polymer Composites 33 (2012) 1071–1076. doi:10.1002/pc.22230.

[45] K. Sever, İsmail H. Tavman, Y. Seki, A. Turgut, M. Omastova, I. Ozdemir, Electrical and mechanical properties of expanded graphite/high density polyethylene nanocomposites, Composites Part B: Engineering 53 (2013) 226–233. doi:10.1016/j.compositesb.2013.04.069.

[46] K. Liu, E. Andablo-Reyes, N. Patil, D. H. Merino, S. Ronca, S. Rastogi, Influence of reduced graphene oxide on the rheological response and chain orientation on shear deformation of high density polyethylene, Polymer 87 (2016) 8–16. doi:10.1016/j.polymer.2016.01.056.

[47] K. Liu, S. Ronca, E. Andablo-Reyes, G. Forte, S. Rastogi, Unique rheological response of ultrahigh molecular weight polyethylenes in the presence of reduced graphene oxide, Macromolecules 48 (2014) 131. doi:10.1021/ma501729y.

[48] W. Zheng, X. Lu, S. Wong, Electrical and mechanical properties of expanded graphite-reinforced high-density polyethylene, Journal of Applied Polymer Science 91 (2004) 2781–2788. doi:10.1002/app.13460.

[49] Z.-K. Chen, J.-P. Yang, Q.-Q. Ni, S.-Y. Fu, Y.-G. Huang, Reinforcement of epoxy resins with multi-walled carbon nanotubes for enhancing cryogenic mechanical properties, Polymer 50 (2009) 4753–4759. doi:10.1016/j.polymer.2009.08.001.

[50] J. Jyoti, B. P. Singh, A. K. Arya, S. R. Dhakate, Dynamic mechanical properties of multiwall carbon nanotube reinforced abs composites and their correlation with entanglement density, adhesion, reinforcement and c factor, RSC Adv. 6 (2016) 3997–4006. doi:10.1039/C5RA25561A.

[51] C. Zeng, S. Lu, L. Song, X. Xiao, J. Gao, L. Pan, Z. He, J. Yu, Enhanced thermal properties in a hybrid graphene–alumina filler for epoxy composites, RSC Adv. 5 (2015) 35773–35782. doi:10.1039/C5RA01967B.

[52] R. Kumar, K. Kar, K. Dasgupta, Static and dynamic mechanical analysis of graphite flake filled phenolic-carbon fabric composites and their correlation with interfacial interaction parameters, Polymer Engineering & Science 58 (2017). doi:10.1002/pen.24809.

[53] W. Pang, J. Wu, Q. Zhang, G. Li, Graphene oxide enhanced, radiation cross-linked, vitamin e stabilized oxidation resistant uhmwpe with high hardness and tensile properties, RSC Advances 7 (2017) 55536–55546. doi:10.1039/C7RA10637H.

[54] A. Borruto, G. Crivellone, F. Marani, Influence of surface wettability on friction and wear tests, Wear 222 (1998) 57–65. doi:10.1016/S0043-1648(98)00256-7.

[55] K. Namachivayam, B. Trindade, N. Emami, Mechanochemical preparation of core-shell structured hydrophobic uhmwpe-onion-like carbon composites, Journal of Molecular Structure 1255 (2022) 132403. doi:10.1016/j.molstruc.2022.132403.

[56] F. Mindivan, A. Çolak, Tribo-material based on a uhmwpe/rgoc biocomposite for using in artificial joints, Journal of Applied Polymer Science 138 (2021) 50768. doi:10.1002/app.50768.

[57] H. Belhamdi, B. Kouini, A. Grasso, C. Scolaro, A. Sili, A. Visco, Tribological behavior of biomedical grade uhmwpe with graphite-based fillers against ebm-ti6al4v pin under various lubricating conditions, Journal of Applied Polymer Science 139 (2022) 52313. doi:10.1002/app.52313.